# Modelling the Greenland Ice Sheet's committed contribution to sea level during the 21st Century

**Isabel J. Nias[1,2,3], Sophie Nowicki[1,4], Denis Felikson[1,5], Bryant Loomis[6]**

[1]Cryospheric Sciences Laboratory, NASA Goddard Space Flight Center, Greenbelt, MD, USA
[2]Earth System Science Interdisciplinary Center, University of Maryland, College Park, MD, USA
[3]School of Environmental Sciences, University of Liverpool, Liverpool, UK
[4]Department of Geology, University at Buffalo, Buffalo, NY, USA
[5]Goddard Earth Sciences Technology and Research Studies and Investigations II, Morgan State University, Baltimore, MD, USA
[6]Geodesy and Geophysics Laboratory, NASA Goddard Space Flight Center, Greenbelt, MD, USA

**Key Points:**

- Glacier terminus position change has a lasting impact on velocity and mass loss of Greenland
- Greenland's committed sea level response by 2100 is comparable to that due to RCP2.6 forcings
- Satellite observations can constrain uncertainty in probabilistic ice sheet model projections

Corresponding author: Isabel Nias, `isabel.nias@liverpool.ac.uk`

## Abstract

Mass loss from the Greenland Ice Sheet can be partitioned between surface mass balance and discharge due to ice dynamics through its marine-terminating outlet glaciers. A perturbation to a glacier terminus (e.g., a calving event) results in both an instantaneous response in velocity and mass loss and a diffusive response due to the evolution of ice thickness over time. This diffusive response means the total impact of a retreat event can take decades to be fully realised. Here we model the committed response of the Greenland Ice Sheet by applying perturbations to the marine-terminating glacier termini that represent recent observed changes, and simulating the response over the 21st Century, while holding the climate forcing constant. The sensitivity of the ice sheet response to model parameter uncertainty is explored within an ensemble framework, and GRACE data is used to constrain the results using a Bayesian calibration approach. We find that the Greenland Ice Sheet's committed contribution to 21st century sea level rise is at least 33.5 [17.5 52.4] mm (25th and 75th percentiles in brackets), with at least 6 mm being attributable directly to terminus retreat that occurred between 2007 and 2015. The spread in our projections is driven by uncertainty in the basal friction coefficient. Our results complement the ISMIP6 Greenland projections, which report the ice sheet response to future forcing, excluding the background response. In this way, we can obtain estimates of Greenland's total contribution to sea level rise in 2100.


## Plain Language Summary

At the edges of the Greenland Ice Sheet are fast-flowing glaciers that flow into the ocean. When the ice front of these glaciers retreat, through iceberg calving and submarine melt, the ice sheet responds both on quick timescales, due to the instantaneous speed up of the ice near the edge, and on longer timescales as the ice dynamics slowly readjust to the initial changes. The slow readjustment of the ice sheet thickness and velocity spreads upstream over time. Therefore, even if climate change (e.g., atmospheric and oceanic warming) was to cease, the ice sheet will continue to respond to changes we have already observed, and will contribute to sea level rise. This contribution is known as "committed sea level rise", which we quantify in this study using a numerical ice sheet model of the Greenland Ice Sheet. We find that glacier retreat between 2007 and 2015 has a lasting impact on ice sheet dynamics by the end of the century and that this should be accounted for in projections of sea level rise.

## 1 Introduction

In recent years there has been a concerted effort within the ice sheet modelling community to produce century-scale projections of sea-level rise from ice sheets under future climate change conditions. The latest international effort comes from the Ice Sheet Model Intercomparison Project for CMIP6 (ISMIP6) (?, ?), which presents multi-model ensembles for the Greenland (?, ?) and Antarctic (?, ?) ice sheets forced by various climate model simulations. The Greenland ISMIP6 results project 90$\pm$50 mm of sea level rise by 2100 under greenhouse gas concentration scenario RCP8.5, and 32$\pm$17 mm for RCP2.6 (?, ?). These values represent the projected ice sheet contribution due to the future climate forcing anomaly, relative to the projection start date of 2015, because values obtained from a control simulation, where climate is held constant, were subtracted from those obtained from the forced simulations. The motivation for this decision was to control for model drift that arises from the initialization process (?, ?, ?); however, subtracting the control simulation also removes any background trend due to changes prior to the projection start date of 2015 (?, ?, ?). The component of sea level rise that is due to these background trends is referred to as the "committed sea level contribution" (?, ?). In other words, regardless of future scenario or climate projection, there is a portion of future sea-level change that is already "locked in" due to the ongoing dynamic response of the ice sheet to past perturbations in marine-glacier termini and the long-term pattern of accumulation and ablation across the ice sheet (surface mass balance, SMB). Modelling the committed sea level contribution of the Greenland Ice Sheet over the 21st century is the focus of this study.

The dynamic component of the committed sea level contribution can be attributed to the varying time scales over which the ice sheet responds to frontal ablation perturbations to marine-terminating glaciers. A retreat event results in an instantaneous adjustment of stresses, causing an increase in the spreading rate of the ice upstream of the terminus or grounding line and the inland extent of the increase in spreading rate is dependent on the geometry (e.g., glacier width) and basal conditions (?, ?, ?). There is also a longer term diffusive response, where thinning propagates upstream due to feedbacks between local geometry, driving stress and velocity (?, ?, ?). This diffusive response is the primary mechanism driving the committed dynamic response because, even if terminus perturbations are halted, the ice sheet will continue to react. Previous work has shown that more than 75% of the total mass loss due to perturbations at the termini of outlet glaciers is due to this long-term diffusive thinning, rather than the instantaneous response to the perturbation (?, ?).

Decreases in SMB since the late 1990s, driven by increases in surface melt, have resulted in SMB becoming the dominant component of the total mass loss, over dynamic discharge through marine terminating glaciers (?, ?, ?). The impact that increased surface melt in the past has on the "committed" contribution to sea level rise in the future is complicated due to various feedback mechanisms. SMB alters the geometry of the ice sheet and enhanced melt can lead to an SMB-elevation feedback where the ice sheet surface lowers as it melts leading to further melt due to the lower altitude (?, ?). Preconditioning of the firn layer, for example through the formation of ice lenses and the associated reduction in percolation and increase in run off, can alter the refreezing capacity of the firn year-on-year (?, ?). However, this process may be more important when considering sea level contributions due to future climate change, as the firn layer loses its ability to buffer high melt rates of the future, rather than the committed response, which is the focus of this paper.

There are several sources of uncertainty to consider in ice sheet projections, including uncertainty in model structure, model parameters, and boundary conditions. It is becoming increasingly common within the ice sheet modelling community to run ensembles of model simulations (?, ?, ?, ?, ?, ?, ?, ?), with the recognition that accounting for uncertainty in a probabilistic way increases the usefulness of projections, despite the intensive computing resources required to produce them. Previous studies have demonstrated that calibration using observations of ice sheet behaviour can help to constrain uncertainty in sea-level rise projections (?, ?, ?, ?, ?, ?).

In this paper, we aim to model the 21st-Century committed response of the Greenland Ice Sheet to observed changes in terminus position of the marine-terminating glaciers, while keeping SMB constant over time. We are motivated by the need for an up-to-date, ice-sheet-wide estimate of committed sea-level rise to aid interpretation of the ISMIP6 projections and guide follow-on efforts. This builds upon the work of ? (?), who modelled the committed response of three of the largest marine-terminating glaciers and then used a simple conceptual model to scale the results up to estimate a Greenland wide value. We use a probabilistic framework to account for model parameter uncertainty and uncertainty in the representation of the present-day SMB by running an ensemble of forward simulations, which we then calibrate using observations of ice sheet mass change from NASA's Gravity Recovery and Climate Experiment (GRACE) mission.

# 2 Methods

## 2.1 Ice Sheet Model

The Ice-sheet and Sea-level System Model (ISSM) is a finite-element ice flow model, which combines conservation laws with constitutive laws and boundary conditions to model ice sheet evolution. The details of how this is implemented can be found in ? (?) – here we will describe the equations relevant to this study.

In this study, we use the shallow-shelf approximation (SSA, ?, ?), also referred to as the shelfy-stream approximation in the ISSM documentation, to model the entire contiguous Greenland Ice Sheet. SSA was chosen because it allowed us to run more simulations at a higher spatial resolution than if we had chosen higher-order physics, and recent literature (?, ?) has shown that sliding dominates even in slow flowing margin regions of the Greenland Ice sheet. Ice is modeled as an incompressible viscous fluid with Glen's flow law (?, ?) used to describe the relationship between the nonlinear depth-averaged effective viscosity and effective strain rate as follows:

$$\mu = \frac{B}{2\dot{\epsilon}_e^{\frac{n-1}{n}}}\,, \tag{1}$$

where $\mu$ is the depth-averaged effective viscosity, $\dot{\epsilon}_e$ is the effective strain rate, $B$ is the depth-averaged ice hardness factor, and Glen's law coefficient $n = 3$. $B$ is found using the temperature-dependent relationship provided by ? (?). In this study we do not solve the thermal model and so the ice temperature, and hence $B$, is kept constant over time. The depth-averaged temperature is taken as the mean temperature at the ice surface from RACMO2.3p2 for 1960-1989 (?, ?). Because the high rate of accumulation and, therefore, the strong downward advection of surface temperature, the upper $\sim 2/3$ of the ice column is at a temperature that is close to the surface temperature. This upper portion of cold ice supports more stress than the lower, warmer portion of the ice column, making our use of the surface temperature as the depth-averaged ice temperature a reasonable assumption. While holding ice temperature constant and estimated from present climate conditions is a simplification, over the timescale of a century this has been shown to have limited impact on ice dynamics, compared to changes basal sliding (?, ?). We also account for uncertainty in the temperature field as part of the ensemble design (see next section).

The basal shear stress is prescribed using a Budd friction law (?, ?):

$$\tau_{\mathbf{b}} = \alpha^2 N \mathbf{u_b}\,, \tag{2}$$

where $\alpha$ is the basal friction coefficient, $\mathbf{u_b}$ is the velocity tangential to the local bed, and the effective pressure $N$ is approximated as $N = g(\rho_i H + \rho_w z_b)$, where $\rho_i$ and $\rho_w$ is the density of ice and ocean water respectively, and $z_b$ is bed elevation, where $z_b = 0$ at sea level and negative below it. Hence, $N$ evolves with geometry and assumes perfect connection between the ocean and any region of the bed below sea level. In reality $N$ is likely to be influenced by subglacial hydrology, but including this factor requires a hydrological model.

The SSA formulation is used to balance the stresses by neglecting vertical shear stresses and bridging effects. The mass transport equation then allows us to update the geometry given mass conservation:

$$\frac{\partial H}{\partial t} = -\nabla \cdot (H\bar{\mathbf{u}}) + \dot{M}_s - \dot{M}_b\,, \tag{3}$$

where $\bar{\mathbf{u}}$ is the depth average horizontal velocity vector, $\dot{M}_s$ is the surface mass balance (m yr$^{-1}$, positive for net accumulation, negative for net ablation) and $\dot{M}_b$ is the basal melting (m yr$^{-1}$, positive for melting). $\dot{M}_b$ is only applied under floating ice tongues.

Hydrostatic pressure is imposed at the front of marine terminating glaciers and no frontal melt or calving law is applied – instead migration of terminus positions is prescribed using a level-set-based method (see experimental design) (?, ?, ?). The grounding line is allowed to migrate using a sub-element scheme (?, ?) and its position is calculated according to hydrostatic equilibrium. We impose a minimum ice thickness of 1 m such that, for any model element that is prescribed to be ice-filled, that element cannot be less than 1 m thick.

The model is initialized to mid-2000s conditions following the method used for the Goddard Space Flight Center (GSFC-ISSM) contribution to ISMIP6 (?, ?). BedMachine v3 geometry (?, ?) and observed surface velocities (?, ?, ?) are used to invert for the basal friction coefficient, following ? (?). A 30-year relaxation is performed using a 1960–1989 mean SMB from RACMO2.3p2 (?, ?). This is to reduce spurious thickness change signals at the start of the forward experiments, rather than to reach a steady state, and therefore dynamic imbalances represented in the initial geometry and velocity derived from the observations are not eliminated.

The model equations are calculated on an unstructured mesh which varies from 25 km resolution in the slow-flowing ice sheet interior, to 500 m resolution in the fastest-flowing outlet glaciers. We impose an additional constraint in which areas that have observed terminus retreat have a resolution of 500 m. This results in a total of about 457,000 mesh elements.

### 2.2 Experimental Design

Forward model simulations start at the beginning of 2007 and run to the end of 2100. We model the impact of recent perturbations to outlet glacier terminus positions by imposing retreat based on observed terminus positions between 2007 and 2015 (?, ?, ?) using a level set method (?, ?). The terminus position dataset provides calving front positions measured during the winter for up to approximately 240 marine terminating glaciers. We assume that the position given by the dataset is stationary between October and May, with retreat occurring linearly over the summer months. Not all years between 2007 and 2015 are represented in the observational terminus position dataset, and therefore we determine missing winter positions by linearly interpolating between two known winter positions. The termini are held at their January 2015 position for the remainder of the century.

Rather than rely on a single model set-up obtained from the initialization process to run our projection, we create an ensemble of simulations with the aim of assessing and accounting for the impact of uncertainty in various model parameters obtained from the inversion (basal friction coefficient) or derived from other models (parameters related to ice viscosity and surface mass balance). The basal friction coefficient field ($\alpha$) is varied uniformly between $\pm 50\%$ of the values obtained by the inversion, because, while the inversion aims to minimize the mismatch between modelled and present-day observed velocities, it is less certain how basal friction changes over time due to processes that can affect sliding, such as hydrology, that we are not accounting for in the model processes. The change is applied as a spatially uniform percentage change, and thus all features described in $\alpha$ obtained from the inversion, for example low friction areas in the narrow outlet glacier channels, are preserved.

The viscosity of the ice is varied through changes in the ice temperature (?, ?), which is applied as an anomaly, with bounds of $\pm 10$K of the temperature used in the initialization, which equals the surface temperatures from RACMO2.3p2 for 1960-1989 (?, ?). We ensure that the temperature does not exceed the melting point anywhere. The depth-averaged ice hardness factor ($B$) is then updated using the temperature-dependent relationship of ? (?), with higher temperatures resulting in softer ice with a lower viscosity. The $\pm 10$K temperature perturbation (with melting point constraint) results in the ice sheet wide mean $B$ varying between -33% and +50% of the unperturbed values used in the initialization.

Surface mass balance is varied in two ways. Firstly, an anomaly is added to the total SMB integrated over the ice sheet, representing the climate variability seen during the 1960-1989 reference period. The standard deviation during this period is 127.5 Gt, which is approximately 30% of the mean SMB over the period. The $\pm$30% of the 1960-89 mean provides the bounds of the anomaly that we apply in the ensemble, which is added uniformly in space to the SMB used in the control run (2001-2015 mean). Secondly, the seasonal amplitude of SMB is varied. The mean seasonal cycle is found for the 1960-1989 period, by finding the mean SMB for each month and then subtracting the annual mean from the monthly means. This is then varied between a factor of 0 (i.e., no seasonal cycle) and 2 (a doubling in the amplitude of the seasonal cycle), and added to the annual mean of the SMB found during the first stage of the SMB perturbation.

The four parameters are sampled using a Latin hypercube design (N=128), and additional simulations are performed using the central member from the initialization and 8 end members where each parameter is varied in turn to its minimum and maximum range, giving an ensemble with 137 members in total (?, ?). Table S1 provides the sampled values for the four parameters for each simulation in the ensemble. The parameter perturbations are applied after the initialization and relaxation procedure, at the start of the 95-year forward simulations. We ran each ensemble member twice: once with observed terminus positions imposed (perturbed simulation) and once with the ice sheet boundary fixed at the initial (i.e., 2007) position (control simulation). Subtracting the mass change simulated by the control simulation from that of the perturbed simulation removes the SMB component of committed sea level rise, as well as ongoing dynamic adjustments from the initial state, both real (because the ice sheet was out of balance in 2007) and artificial (i.e. erroneous model drift). In this study, we use "total committed sea level rise" to mean the total sea level contribution from the perturbed simulation and "dynamic committed sea level rise" to mean the contribution after the control simulation is removed and therefore is in direct response to the imposed retreat. To calculate the total GrIS contribution to future sea level rise, total committed sea level rise must be added to the ISMIP6 anomaly projections. The dynamic committed sea level rise, on the other hand, is useful for understanding the direct impact that recent retreat of marine terminating glaciers has on ice flow dynamics over the coming decades.

### 2.3 Bayesian Calibration

The parameter sampling described in the previous section was intentionally conservative, thus producing a broad distribution of committed sea level rise (red curve, Fig. **??**). To reduce the spread, we perform a Bayesian calibration that weights each ensemble member based on its ability to reproduce observed mass change. To do this we use a regularized mascon solution derived from the Gravity Recovery and Climate Experiment (GRACE) Level 1B data described by ? (?), which provides total mass change between 1 January 2007 and 1 January 2015 in each mascon area, with a spatial resolution of 1-arc degree ($\approx$115 km) (Fig. **??**a). Because of signal leakage between the mascons, the regularized solution may be biased and the resulting leakage errors are determined by a resolution operator, $\mathbf{R}$, which can be used to relate the unknown truth state, $\mathbf{x}$ to the estimated state, $\hat{\mathbf{x}}$, via $\hat{\mathbf{x}} = \mathbf{R}\mathbf{x}$ (?, ?, ?). Therefore, in order to compare like-for-like between the GRACE mascon observations and the model output, we first aggregate the modelled mass loss over the same period into the same spatial bins as the mascons and then apply the resolution operator. In a sense, this is like we are assuming the model is the truth ($\mathbf{x}$), and multiplying by the resolution operator given the "GRACE-view" estimate ($\hat{\mathbf{x}}$).

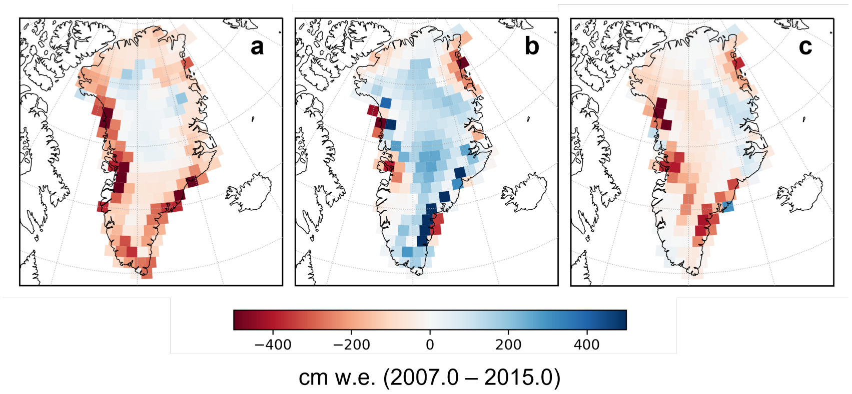


**Figure 1.** Mass change between January 2007 and January 2015 from GRACE mascons observations (a) and from low (b) and high (c) weighted ensemble members converted into "GRACE-view" mascon estimates ($\hat{\mathbf{x}}$).

Similarly to (?, ?), we calculate a likelihood score $s_j$ for each ensemble member $j$ based on the discrepancies between modeled and observed mass loss:

$$s_j = \exp\left[-\frac{1}{2}\sum_i \frac{(f_i^j - z_i^j)^2}{(\sigma_i)^2}\right], \tag{4}$$

where $f$ is the modelled and $z$ is the observed mass loss, and $i$ is an index of the basin. We aggregate the mass loss on a basin scale using the basins outlines described by ? (?) – this helps ensure the model-observation discrepancies are spatially uncorrelated. Semi-variograms of the model-observation discrepancies show that there is some correlation between discrepancies that are closer than 200-300 km, therefore calculating discrepancies on the individual mascon scale is inappropriate (?, ?).

Observational and model structural error ($\sigma_o^2$ and $\sigma_m^2$) are accounted for in the discrepancy variance, $\sigma^2$, such that $\sigma^2 = \sigma_o^2 + \sigma_m^2$ (?, ?). This provides some leniency to the score calculation – ensemble members are not overly penalised for a mismatch between the modelled and observed mass loss, given that these quantities have errors associated with them that are not sampled by the ensemble. GRACE measurement uncertainties are determined by examining the statistics of the differences between the high-resolution mascon trend solution (?, ?) and the GOCO-06 spherical harmonic model (?, ?). There are many sources of error related to the structure of the model (e.g., numerical representation of processes, missed processes, grid and time-step resolution), which are difficult to quantify. Therefore here we test a range of values estimated by multiplying the observational error by a factor of 2, 4 and 8, and, in doing so, we are stating that our confidence in our ability to model reality is lower than our ability to measure it (?, ?, ?, ?). The resulting scores are normalised to created weights ($w_j = s_j / \sum j(s_j)$) that are then used to produce the posterior probability density functions.

## 3 Results

Table **??** shows the quantile and modal estimates of sea level contribution by 2100 relative to the start date. The ensemble of model simulations results in a prior estimate of 21.6 [-13.1 83.7] mm total sea level rise, expressed as sea level equivalent (SLE, median [25th 75th percentile]; estimated from the empirical cumulative density functions using bootstrapping, with a sample of N=10000 (?, ?)) by 2100 (red prior curve, Fig. **??**). The calibration procedure shifts the median of the distribution to higher values of

**Table 1.** Quantiles and mode from prior and posterior distributions of sea level contribution (mm SLE) by the end of 2100 relative to the beginning of 2007 and 2015 (i.e., the ISMIP6 projection period).

| | | 5% | 25% | 50% | 75% | 95% | Mode |
|---|---|---|---|---|---|---|---|
| Total committed sea level rise [a] 2007–2100 | Prior | -44.8 | -13.1 | 21.6 | 83.7 | 206.4 | -7.9 |
| | Posterior, $\sigma_m = 4\sigma_o$ | 16.0 | 29.6 | 38.6 | 51.6 | 59.8 | 39.5 |
| | Posterior, $\sigma_m = 8\sigma_o$ | -12.0 | 17.5 | 33.5 | 52.4 | 76.2 | 34.8 |
| Dynamic committed sea level rise [b] 2007–2100 | Prior | 3.9 | 4.6 | 6.2 | 8.3 | 12.1 | 4.9 |
| | Posterior, $\sigma_m = 4\sigma_o$ | 5.4 | 6.2 | 6.4 | 7.0 | 8.2 | 6.6 |
| | Posterior, $\sigma_m = 8\sigma_o$ | 4.5 | 5.7 | 6.3 | 7.0 | 8.3 | 6.4 |
| Total committed sea level rise [a] 2015–2100 | Prior | -42.1 | -13.6 | 19.1 | 77.0 | 191.0 | -6.9 |
| | Posterior, $\sigma_m = 4\sigma_o$ | 12.6 | 25.4 | 35.1 | 46.0 | 53.7 | 35.0 |
| | Posterior, $\sigma_m = 8\sigma_o$ | -11.9 | 15.8 | 31.4 | 48.9 | 70.2 | 31.5 |

[a]Perturbed simulations.
[b]Perturbed - control simulations.

sea level contribution and narrows the interquartile range; for example, in the case where we estimate structural error to be a factor of 8 greater than the observational error ($\sigma_m = 8\sigma_o$), the posterior distribution results in 33.5 [17.5 52.4] mm SLE by 2100. The posterior distribution is sensitive to the magnitude of the structural error estimate, with a higher structural error (and therefore discrepancy variance) resulting in a shorter and broader peak (grey posterior curves, Fig. **??**). In the case where the structural error is assumed to be double the GRACE measurement error, the scores are heavily weighted to a small number of ensemble members, producing a sharp peak and estimating the percentiles using a empirical cumulative density function becomes less reliable. When more leniency is allowed in the model-observation discrepancy (i.e., when the discrepancy variance is higher), the weights are more evenly distributed and, thus, a broader posterior distribution is obtained. Table S1 provides the calibration weights for each simulation in the ensemble at various discrepancy variances that we tested.

By subtracting the control simulations from perturbed simulations, we find that the perturbations in terminus positions between 2007 and 2015 result in 6.3 [5.7 7.0] mm SLE of dynamic committed sea level rise by 2100 (when $\sigma_m = 8\sigma_o$). The rate is highest towards the beginning of the simulations after the period of most sustained retreat between 2010 and 2013 (Fig. **??**). After 2015, the rate decreases but remains positive for the duration of the simulations, indicating that ice sheet flow will continue to adjust to the terminus perturbations of the recent past, even beyond 2100. Subtracting the control simulations gives us the dynamic portion of the committed response that is directly attributed to the perturbations at the ice front, which allows us to compare with the results of ? (?).

In the ensemble, the pattern of sea level response is primarily driven by the variation in basal friction coefficient and the central values, closest to the coefficient obtained by the data assimilation process, are weighted highly compared to the extremes of its distribution (Fig. **??**). This indicates that the data assimilation process, in which we seek to minimize the misfit between observed and modelled velocity by tuning the basal friction coefficient, yields simulations with modeled mass changes that are in better agreement with independent observations from GRACE. Secondary to the variation in basal sliding, the simulations with higher ice temperature, and therefore less viscous ice, are more likely to have a higher weight in the calibrated ensemble than those with colder,

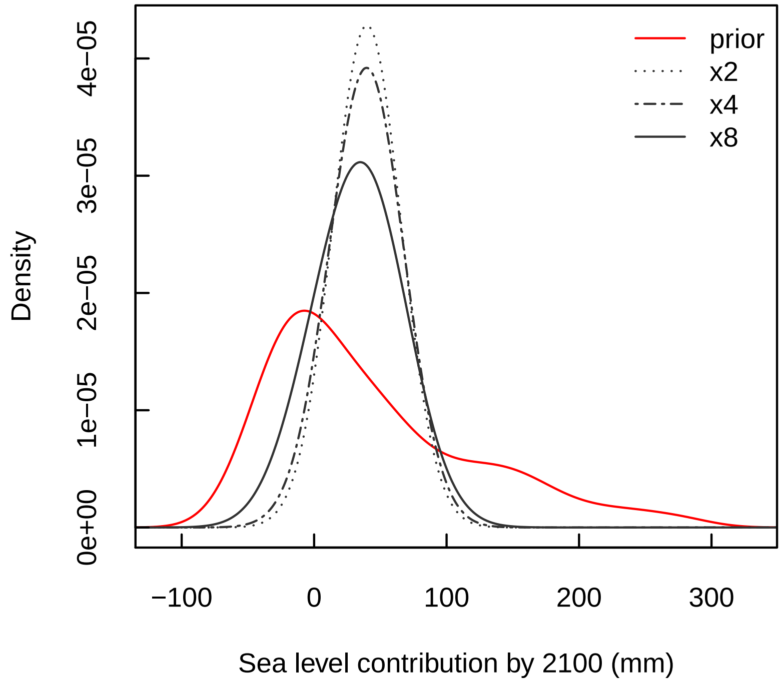


**Figure 2.** Prior (red curve) and posterior (grey curves) probability density functions of the total committed sea level rise by 2100. The control has not been removed and so this signal includes mass change due to the dynamics and the SMB trend. Different values for the structural error have been tested by multiplying the measurement error by 2, 4 or 8.

more viscous ice. The ensemble members with higher ice temperature result in higher sea level response, although there are still ensemble members with high sea level response and low ice temperatures, due a lower basal friction coefficient. There is a slight tendency for ensemble members with a more negative SMB anomaly to have a higher sea level contribution, but variability in the strength of the seasonal cycle in SMB has no discernible impact on the calibration or the committed sea level contribution. Ensemble members with both high and low sea level response can be found at all values of both SMB anomaly and SMB seasonality and the high-weighted ensemble members are spread throughout the full range of values for these parameters.

## 4 Discussion

Retreat events in the early 2000s continue to affect ice dynamics at the end of the century and, although the impact diminishes the more distant the retreat event is in the past (Fig. **??**), the rate of ice mass loss in the perturbed simulations remains elevated above the control simulations throughout the 21st century. A similar result is reported by ? (?), who argue that the sea level response in the three years following a perturbation can be attributed to the perturbation itself, after which the sea level contribution is instead due to the long-term, diffusive thinning of the ice sheet. They find that the long-term diffusive behaviour is responsible for $\geq$75% for the total sea level contribution

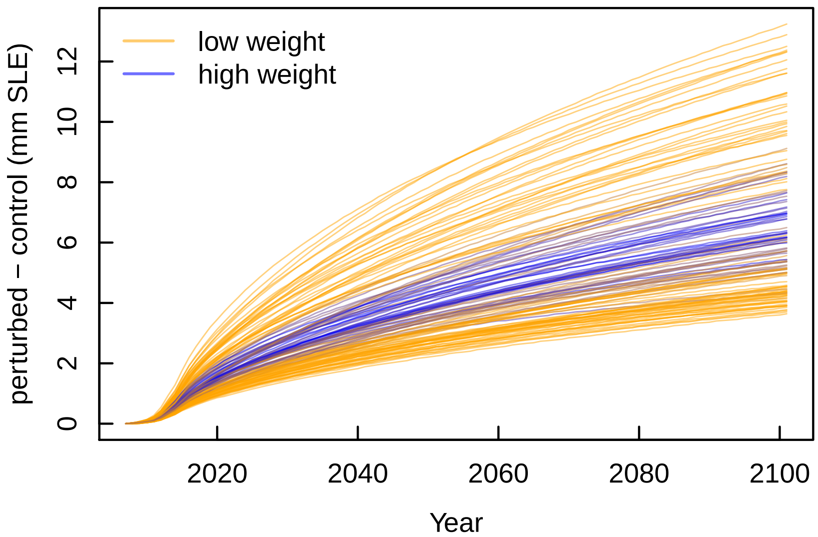


**Figure 3.** Dynamic committed sea level rise from model ensemble (N=137). Blue colours indicate the highest weighted ensemble members when calibrated with GRACE observation (where $\sigma_m = 8\sigma_o$).

after 100 years. Using the same metric here, approximately 80% of the total sea level contribution in 2100 is due to the diffusive response to the initial perturbations. Our estimate of the dynamic committed sea level contribution between 2007 and 2100 (6.3 [5.7 7.0] mm SLE) is also very similar to that of ? (?), who estimated 6.0±2.0 mm SLE between 2000 and 2100, despite the differences in modelling approaches.

The short lived period of retreat results in an initial increase in flow speed near the terminus and in the main channel of tidewater glaciers, increasing the flux across the terminus. The acceleration in flow speeds and resulting longitudinal stretching causes the ice surface to lower, which then propagates upstream, giving rise to dynamic thinning. The velocity of the perturbed simulations remain elevated above that of the control simulations (Fig. **??**), although the acceleration slows over the course of the experiment. The thinning signal diffuses upstream and dissipates, as the ice sheet geometry approaches a new state of balance, with an increased velocity required to maintain the same flux (assuming no change in SMB) due to the reduction in thickness (Fig. **??**). We note that while we ended our experiments in 2100, in line with the ISMIP6 projections, the ice sheet does not reach equilibrium in this time, and we expect it to continue to respond to the changes in the following centuries.

The dynamic committed response of the ice sheet, and the uncertainty associated with the estimates, has regional differences. Figure **??** shows the 2100 dynamic sea level contribution for each of the major Greenland basins that is directly caused by the imposed retreat (?, ?, ?). The Southwest (SW) is dominated by land terminating glaciers, rather than tidewater glaciers, and therefore has experienced limited terminus retreat, leading to a limited sea level response. However, it does not necessarily follow that the basins that experienced the most terminus retreat by area go on to contribute the most to sea level due to that retreat. For example, the Northern (NO) region experienced the second highest amount of retreat between 2007 and 2015 (approximately 520 km$^2$, ? (?)), but has the lowest median dynamic committed response. This region is home to Petermann Glacier, which has the largest remaining floating tongue in Greenland. During the 2007–2015 perturbation period, the floating tongue experienced large calving events that

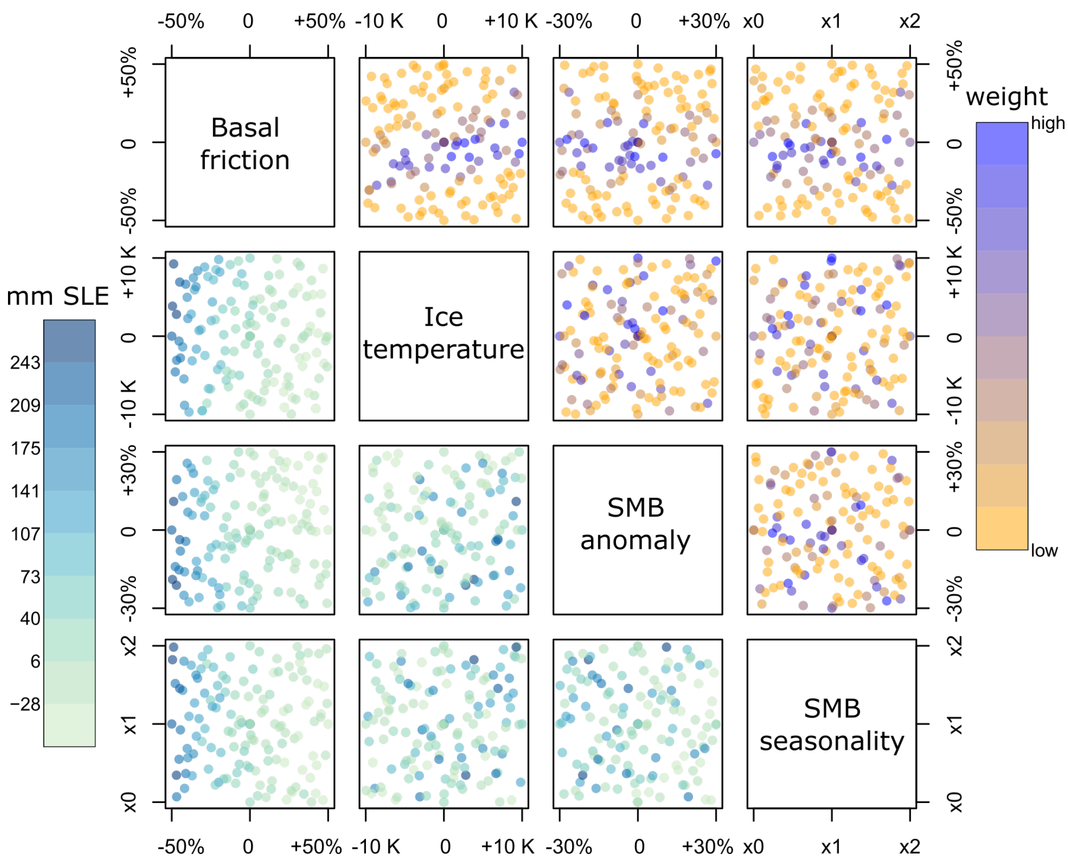


**Figure 4.** Interactions between the parameters varied within the ensemble framework. In each panel, the symbols represent individual ensemble members within the parameter space, coloured to indicate weights from the GRACE calibration with $\sigma_m = 8\sigma_o$ (top-right panels) and the total committed sea level contribution by 2100 (bottom-left panels). The axis labels indicate how each parameter is varied in relation to the central ensemble member derived from the initialization.

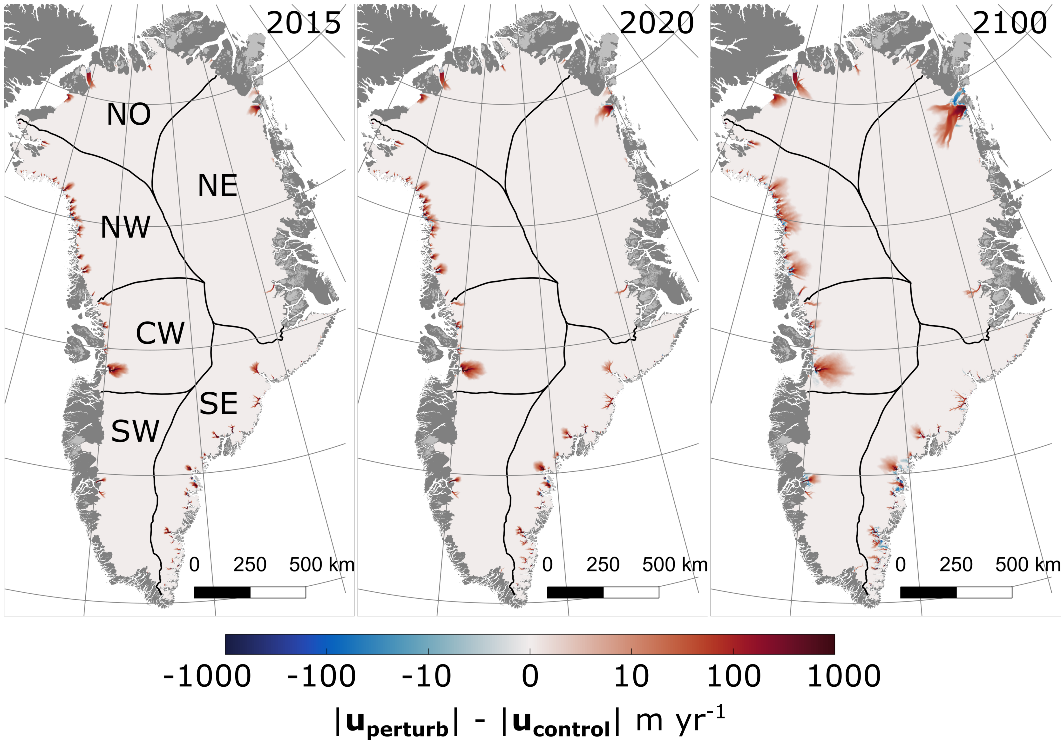


**Figure 5.** Difference in ice surface velocity between a perturbed simulation and its respective control simulation at 2015, 2020, 2100 for a highly weighted ensemble member.

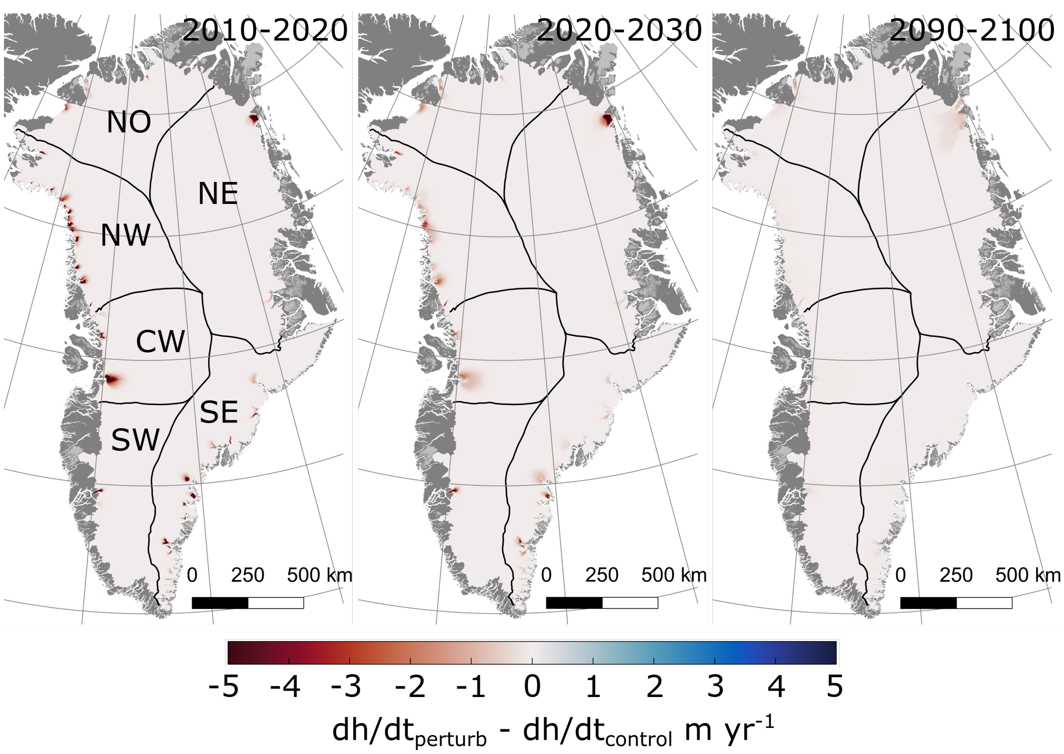


**Figure 6.** Difference in thinning rates between a perturbed simulation and its respective control simulation averaged over the ten years leading up to 2020, 2030 and 2100 for a highly weighted ensemble member.

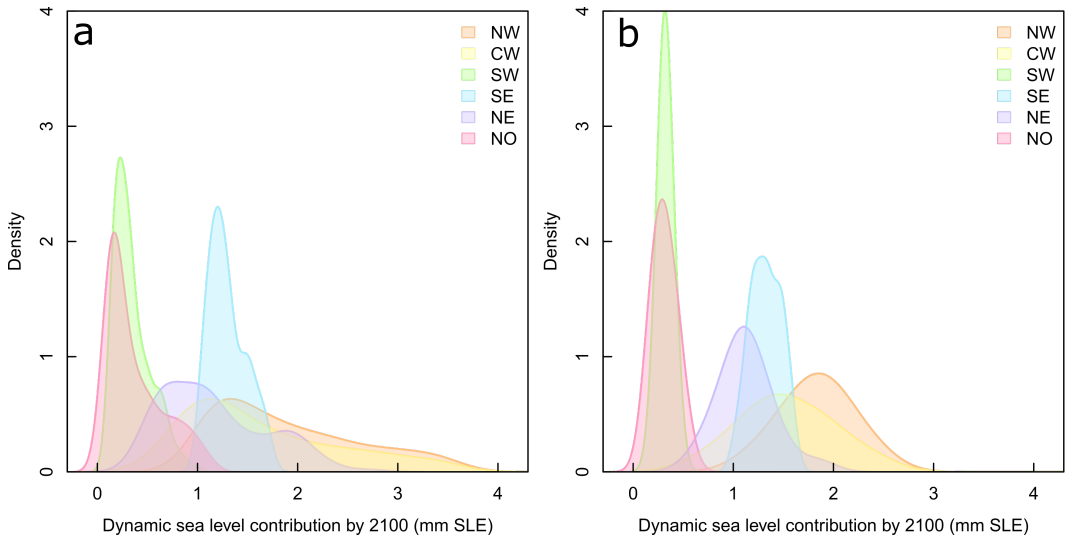


**Figure 7.** Dynamic sea level contribution (perturbed - control) by 2100 for each drainage basin: (a) the prior and (b) the calibrated posterior (with $\sigma_m = 8\sigma_o$) probability density functions.

made up two thirds of the total retreat area experienced by the region. However, it appears that these calving events have minimal impact on the glacier thinning rates (Fig. **??**), indicating that the region that calved from the floating tongue did not provide significant buttressing to the upstream ice – i.e., it is a passive ice shelf (?, ?). Similar results have been demonstrated by ? (?), who found that the floating tongue only provides buttressing within 12 km of the grounding line, where thick ice is close enough to the grounding line such that, if floating ice is removed, the stresses at the grounding line are affected. Another major glacier in the NO region, Humboldt Glacier retreated by 89.5 km$^2$ during the perturbation period. However, it is a slow moving glacier (?, ?) and therefore in absolute terms the impact of any acceleration it experienced on the dynamic response is also limited.

The Northwest (NW) and Central West (CW) have the highest medians and upper bounds of dynamic sea level contributions as a result of the retreat they experienced between 2007–2015 (Fig. **??**). The NW experienced the third highest total area of retreat between 2007 and 2015 (365 km$^2$) across many ($\sim$70) marine terminating glacier fronts, whereas the CW has experienced only 81 km$^2$ of retreat, 40% of which is attributed to Jakobshavn Isbræ. Over the course of the simulation, the acceleration of Jakobshavn Isbræ relative to the control spreads 100s km upstream, sustaining an elevated rate of sea level contribution over the century.

The Northeast region (NE) experienced the most retreat during the perturbation period (930 km$^2$), with approximately 90% due to retreat of the ice shelf of ZachariæIsstrøm – one of the outlet glaciers fed by the Northeast Greenland Ice Stream (NEGIS). Compared to the NO glaciers, the retreat of the floating ice in the NE has a greater impact on the sea level response. Compared to the other regions, a higher proportion of the response by 2100 is due to the long-term diffusive behaviour, with 91% of the sea level response occurring more than three years after the end of the retreat perturbation. In part, this is because the initial removal of ice does not directly contribute to sea level as it is already floating, however it also has a lasting impact on the upstream velocity of NEGIS (Fig. **??**) and the elevated rate of negative surface elevation change persists for longer than other glaciers (Fig. **??**).

Retreat of marine terminating glaciers in the Southeast (SE) results in a high contribution to sea level, but the range across the ensemble is low compared to the other high contributing regions, such as the NW and CW (Fig **??**). This suggests that the glaciers in the SE, which tend to reside on steep mountainous terrain, are less sensitive to the model parameters perturbed in the ensemble, compared to glaciers on gentler bedrock gradients in the NW and CW. This has implications for projections as the regions of gentle sloping topography have the potential to cause high amounts of sea level rise because diffusive thinning is able to spread to the interior of the the ice sheet (?, ?, ?), but the certainty in their behaviour is poorly constrained. An example of a difference in the sensitivity between glaciers in the SE and NW are shown in Figure **??**, where the spread of ensemble members is greater for Kakivfaat Sermiat in the NW, compared to Helheim Glacier in the SE. The spread in responses is driven by uncertainty in the basal conditions (i.e. sliding). The steep topography in the SE helps restrict the upstream influence of retreat events to the lower reaches of the glaciers (?, ?), and we find that the proportion of the response that is due to the long-term diffusive behaviour is lower for the SE ( 71%) compared to other regions (e.g., 91% in the NW). This difference in uncertainty of response is also demonstrated by longer term projections of the Greenland Ice Sheet, where the likely range in the projected retreat is larger in the North and West compared to the SE (?, ?).

Our estimate of the total committed contribution to sea level rise between 2015 and 2100 (Table **??**) can be added to the ISMIP6 projections of GrIS response to future climate anomalies to obtain the total estimated sea level rise from the GrIS over the 21st century. ISMIP6 projects 90±50 mm of sea level rise from GrIS by 2100, relative to 2015, under RCP8.5, and 32±17 mm SLE for RCP2.6 (?, ?). These projections use atmospheric and oceanic anomalies acquired from selected CMIP5 models to force the ice sheet models under RCP scenarios – when the ice sheet models are forced with a selection of CMIP6 models, the sea level contribution tend to be higher by up to a factor of two for the equivalent SSP (?, ?): for SSP5-8.5, the contribution by 2100 is projected to be 80-250 mm SLE relative to 2015, and for SSP1-2.6, 20-60 mm SLE (?, ?). As expected, the ISMIP6 projections under the high emissions scenarios (RCP8.5/SSP5-8.5) are considerably higher than our estimates of total committed sea level contribution because the changes in climate we expect over the 21st century according to the CMIP models result in a greater ice sheet anomaly than the current signal (i.e., surface mass balance will become considerably more negative than present). However, under the lower emissions scenario (RCP2.6), GrIS's sea level contribution by 2100 due to forcing anomalies is approximately equal to its estimated total committed sea level contribution. We note that in the latest Assessment Report from the Intergovernmental Panel on Climate Change (IPCC AR6), 20±10 mm SLE was added to the 2100 sea level contribution (relative to 2015) reported by ISMIP6 to account for the removal of the control simulations in ISMIP6 (?, ?), which is similar to our estimates for the ISMIP6 projection period, for example 31.5 [15.8 48.9] mm SLE when $\sigma_m = 8\sigma_o$ (Table **??**).

Between 15 and 20% of the total committed sea level response can be attributed to the retreat of marine terminating glaciers, and the rest is due to the prescribed SMB and the transient dynamic response to this, as well as ongoing stress balance adjustments, some of which may be artificial (i.e., model drift). Distinguishing between these various contributors to the overall trend is difficult and, while our results demonstrate that the committed response should be accounted for in projections of sea level rise, producing an accurate representation of this, which avoids the issues of model drift, is not straightforward. For example, the committed sea level results are likely to be sensitive to the choice of SMB field that is held constant for the duration of the simulations. Here we purposely used a temporally averaged field (2001-2015) in order to smooth out extreme years, but choosing a different SMB product or time period would likely result in a different result. A recent SMB model intercomparison project found that estimates of past SMB have a wide spread (?, ?), with a standard deviation of the 1981–2012 mean SMB

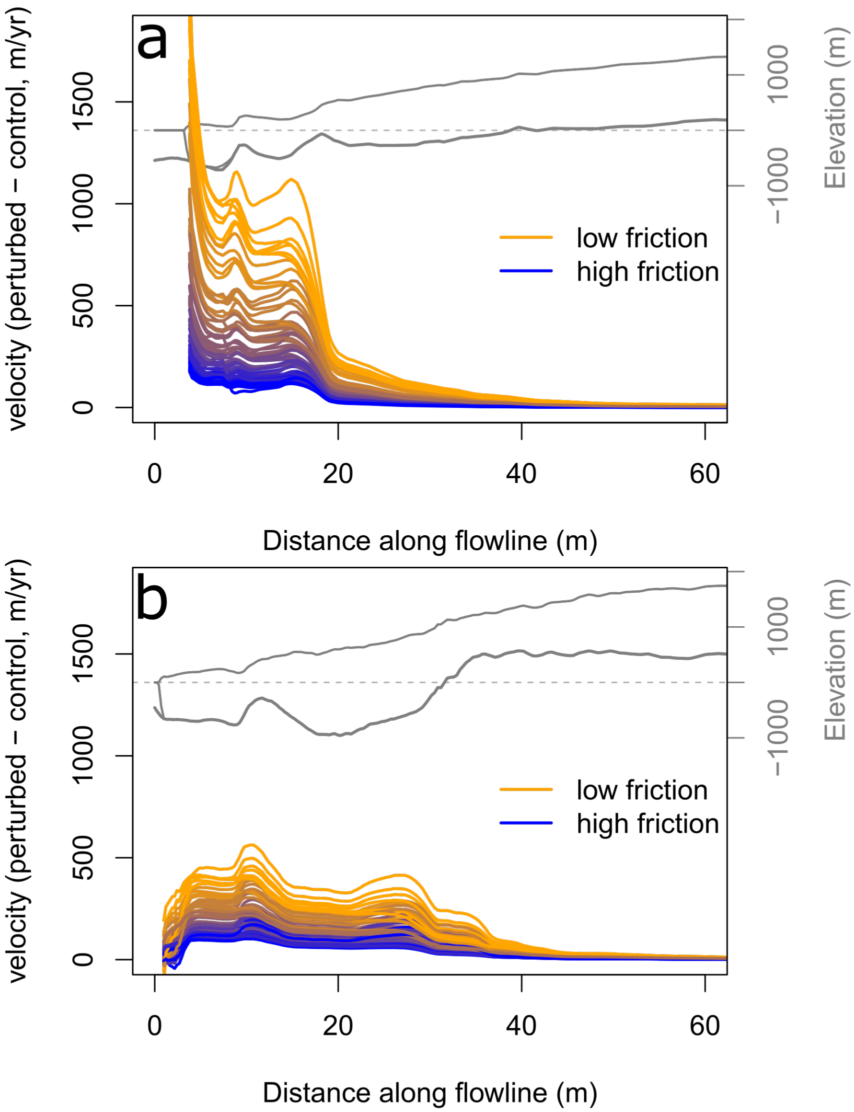


**Figure 8.** Difference in ice surface velocity between perturbed simulations and their respective control simulation at 2100 for flowline along a) Kakivfaat Sermiat, NW and b) Helheim Glacier, SE. Blue curves represent ensemble members with higher basal friction and orange curves represent those with lower basal friction. Geometry (ice surface, base and bedrock elevation) along flowline shown in grey.

across all models of approximately 27% of the mean, which we note is similar to the range that we varied SMB over in our ensemble (up to ±30% of the 2001-2015 mean). However, the spread between SMB models is particularly wide at the margins (?, ?), but we did not test for differences in the spatial pattern of accumulation and ablation.

Ideally, the need to subtract a control to remove biases due to model drift would be eliminated in future ISMIP-style community efforts through improvements in the consistency of input data and initialization methods, so that we are better able to capture the initial state and trends of the recent past (?, ?). Nevertheless, uncertainties will remain and certain aspects of the uncertainty can be explored using perturbed-parameter ensemble approaches. This method, however, is time consuming and computationally expensive, and therefore a large community-led activity such as ISMIP would benefit from a more targeted approach where only the most sensitive and poorly constrained parameters are varied within the ensemble, thereby reducing the necessary number of ensemble members. A related approach that future ISMIP-style efforts would benefit from is to perform a Bayesian calibration of the perturbed-parameter ensemble using observations of past change, similar to the approach taken here (?, ?). Bayesian calibration should reduce the problem of model drift because the simulations that best match the historical period are more highly weighted, and therefore simulations that exhibit real transient signals in the ice sheet system are preferentially represented over simulations where the trends are dominated by artificial model drift.

An inherent limitation of calibration using observations is that it is limited by the length of the observational period – in this case we calibrate with just eight years, which is very short compared to the response times of ice sheets. Ensemble members that perform similarly well during the calibration period (2007-2015) can diverge from one another during the projection period (2015-2100), which limits the constraint that the calibration can have on the 2100 posterior distribution, although we note that Figure **??** demonstrates that the relationship between different ensemble members is mostly consistent over time. In addition to the parameter uncertainty explored here, there may also be biases due to the choice of model physics. We use SSA in this ensemble to reduce computational costs of running an ensemble at a high spatial resolution and because sliding dominates for outlet glaciers, to which we applied retreat perturbations. We repeated the initialization process followed by a small number of ensemble members using higher-order physics and they produce a lower dynamic response to the retreat perturbations than SSA (Text S1, Supplementary Information). SSA does not allow for ice flow due to internal deformation, and this is therefore compensated for by the basal friction coefficient derived during the inversion. This means that the SSA simulations more efficiently transfer stresses to the slower flowing interior regions in response to perturbations at the outlet glacier termini. This leads to higher mass loss for simulations run with SSA physics than those run with higher-order physics, with all other model parameters and forcings the same. While the calibration approach can ensure that the posterior is consistent during the calibration period, the impact of any biases and uncertainties are likely to grow over time.

In addition to the SSA momentum-balance approximation, our simulations of the GrIS use the assumption that depth-averaged ice temperature is equal to the average surface temperature between 1960 and 1989. This ice temperature is used to obtain ice viscosity, which is held fixed through time for each simulation and we sample uncertainty in ice viscosity as part of our ensemble. However, future work could build on our results by performing additional simulations to test other approximations of depth-averaged ice temperatures and quantify the impact of these various assumptions. For example, an analytical solution for the vertical profile of ice temperature can be obtained and averaged over the depth to obtain a spatially varying estimate of depth-averaged ice temperature (?, ?). Alternatively, a vertically integrated temperature that is consistent with the SSA approximation can be used to obtain depth-averaged ice temperature (?, ?). New simulations using these approximations of depth-averaged ice temperature could be performed to quantify the impact of ice viscosity on the projections.

There is no formal definition of committed sea level rise from ice sheets, and we acknowledge that by focusing on terminus retreat only it is likely that the definition used here is a lower bound. For example, there are various feedbacks related to SMB, such as with ice sheet surface elevation and albedo, which could exacerbate mass loss over the century without any additional climate forcing, which we do not account for. SMB has been changing for several decades prior to the start of our experiments (?, ?). However, this change is represented in our model in the geometry product used in the initialization, i.e. accumulation and ablation changes prior to the 2007 initial state contributes to the form of the surface slope, which impacts ice dynamics through the driving stress. Additionally, we hypothesize that initializing the model further back in time and performing the calibration over a longer historical period would likely do a better job at capturing the ice sheet state and tendencies in 2015. However, by forcing the model with terminus position changes during the 2007–2015 calibration period ensures that we are capturing the ice sheet's committed mass loss in direct response to the prescribed retreat. ~~However~~Nevertheless, some antecedent conditions that are not included in our model could enhance mass loss through SMB and ice sheet dynamics, for example refreezing of melt water in the firn layer resulting in excess surface runoff (?, ?). The ongoing development of coupled ice-sheet-climate models is critical for incorporating missing processes and feedbacks into sea level rise projections (?, ?).

## 5 Conclusion

We performed an ensemble of 137 Greenland Ice Sheet simulations, where we varied parameters related to basal friction, ice temperature and surface mass balance, and imposed terminus positions based on changes observed between 2007 and 2015. The ensemble members were then run until the end of the 21st century. We found that, after performing Bayesian calibration using GRACE observations, the Greenland Ice Sheet's committed sea level contribution by 2100 is at least 33.5 [17.5 52.4] mm SLE (median [25th 75th percentile]), with at least 6.3 [5.7 7.0] mm SLE due to the dynamic response to the retreat of marine terminating glaciers at the beginning of the simulations. The spread of responses in the ensemble is driven by the basal friction coefficient, which exerts the greatest control on modelled mass loss. As a result, the GRACE calibration has the greatest impact on constraining the parameter range of the basal friction coefficient, compared to other parameters, with the central members, close to or slightly lower (i.e., more slippery) than the basal friction coefficient field produced by the inversion, being the most highly weighted. Ice temperature has a limited impact on the spread of ice sheet response, although we find that warmer ice (and hence less viscous ice) produces a better match with GRACE observation, for similar reasons that more slippery beds better match with observations: our initial state, which serves at the central member of our ensemble, underestimates mass loss. The spread in the SMB perturbations is not well constrained by GRACE observations, although this is likely due to the way the anomaly was implemented uniformly across the ice sheet.

There is variation in how regions respond to retreat of their marine terminating glaciers. Retreat in the NW, NE, CW and SE result produce the highest response, relative to the control, although the SE has a narrower spread in response across the ensemble, indicating that some regions are less sensitive to basal sliding than other regions. The dominant geometric configuration of outlet glaciers in the different regions is likely to be an important factor in their response to terminus retreat, as indicated by the findings of ? (?) – for example the gentle sloping topography in the NW, CW and NE allows the thinning signal to spread far inland.

According to the results of our calibrated ensemble, the total committed sea level contribution by the end of the century is comparable in magnitude to the contribution due to future climate anomalies under the RCP2.6 scenario. Under the higher emission scenario of RCP8.5, the contribution due to future forcing is approximately a factor of three higher than the committed response. Our results highlight the importance in working towards multi-model ensembles where the need to remove a control run can be avoided. One potential solution is to use a Bayesian calibration process, as was done here, to improve our confidence in the model's ability to reproduce a historical period, while minimising the impact of model drift.

**Acknowledgments**

The authors were supported by research grants from the NASA Sea Level Change Team, the NASA Cryosphere Program and the NASA Modeling and Analysis Program. In addition, DF was supported by an appointment to the NASA Post-doctoral Program at the NASA Goddard Space Flight Center, administered by Universities Space Research Association under contract with NASA. ISSM is open source software that can be downloaded from https://issm.jpl.nasa.gov. ISSM version 4.16 was used in this study. Ice surface velocity, geometry and terminus positions are available at the National Snow and Ice Data Center (https://nsidc.org/). RACMO2.3p2 FGRN055 data can be accessed at https://www.projects.science.uu.nl/iceclimate/models/racmo-data.php. The monthly GRACE mascon products used in this study can be accessed at http://neptune.gsfc.nasa.gov/grace. We acknowledge the contributions of Kenneth Rachlin to the GRACE data processing system. We are grateful to Beata Csatho for the helpful discussions about this work.